Controller Gain Selection for Microgrids with Multiple Operating Modes

T. Roberts, S. Rajnarayanan, and A. D. Domínguez-García
Department of Electrical and Computer Engineering
University of Illinois at Urbana-Champaign, Urbana, IL 61801, U.S.A
Email: {tgr2, sr115, aledan}@illinois.edu

***Abstract*—This paper examines closed-loop stability of a radial microgrid with nine controllers. The microgrid is equipped with heterogeneous generation sources which can operate in parallel (in grid connected, backfed, or networked mode) or independently (in partially or fully islanded mode). Feeder 1 comprises a diesel generator (DG) and feeder 2 comprises a droop-based grid forming (GFM) inverter. A linearized state-space model is used to determine how gain choice affects stability of the full-order system throughout seven distinct topological modes with various controls enabled. Controls include regulation of frequency, voltage, active power, reactive power, and the synchronization of islanded feeders to the grid/one another. The linearized state-space model encompasses all possible controls in all possible modes, and is used to (numerically) examine regions of stability/instability.**

***Index Terms*—microgrids, control system design, gain selection, stability analysis, controller hardware in the loop.**

I. Introduction

MICROGRIDS are often required to be operationally flexible and operate in different modes/topologies such as grid connected, islanded, networked, or backfed mode. Additionally, microgrids often have the added complication of having heterogeneous generation such as diesel generators (DGs) and grid forming (GFM) inverters that must operate in parallel. A suite of controllers is generally responsible for seamlessly transitioning between modes as well as regulating voltage and frequency. Therefore, it is imperative to choose stable gains for each of the modes in which the microgrid can operate and a multitude of possible controls that may or may not be active at a given time. However, it is difficult to tune controllers and determine regions of stability for such nonlinear and multi-mode systems.

In order to showcase our approach, we adopt, as a starting point, the Banshee microgrid, a radial three feeder heterogeneous microgrid [1], which we emulate using high-fidelity component models in real-time in a controller hardware-in-the-loop (C-HIL) environment. To simplify the developments, we examine an abridged version of Banshee comprising feeders 1 and 2 of the original system. The two-feeders can be connected to one another in various topologies that we call modes, and the system comprises a suite of nine controllers. These controllers ensure seamless transitions between modes and regulate key quantities in the system such as frequency, voltage, active power, and reactive power. In order to analyze stability of the system and its numerous controls and choose controller gains, we derive a linearized state-space model of the abridged system. This in turn helps us tune the gains of the high-fidelity model emulated in the C-HIL lab.

While many recent works have examined secondary frequency and secondary voltage control within microgrids, works that examine islanding and re-synchronizing feeders from/to the grid are less common [2]–[6]. Furthermore, while some works specify that the controls for the system must be tuned, and/or give simple conditions on stability [5], [6], they do not discuss how the controls are tuned. However, in [2] the authors present an optimization-based control algorithm when the microgrid is islanded or grid connected. Based on our literature review, and to the best of our knowledge, limited work has been done on tuning microgrid controllers across multiple modes such as those we present here.

II. System Models

In this paper, we adopt the Banshee system—a radial three-feeder microgrid that "resemble[s] emerging microgrids around the world, making it a comprehensive benchmark to evaluate microgrid performance" [1]. In this section, we first present an abridged version of the complete Banshee system comprising feeders 1 and 2 of the original system. Then we present a linearized model used to analytically tune controller gains for the full-order system model.

A. The Abridged Banshee System

Figure 1 depicts an abridged version of the Banshee microgrid, that comprises feeders 1 and 2 of the original three-feeder system, which was introduced in [1]. This model includes the bulk grid modeled as an infinite bus, 17 buses, 11 constant impedance loads totaling 5,070 kVA, 33 CBs, 3 Schweitzer Engineering Laboratory (SEL) relays, and 2 generating resources. Each of the three SEL relays controls a CB (CB000, CB100, CB200), and CB000 is the point of interconnection (POI) with the grid. The status of certain CBs is normally open (NO), while the status of others is normally closed (NC), as identified in Fig. 1.

A high-fidelity model of the Banshee system is implemented on Typhoon HIL real-time hardware devices, and comprises detailed generator models, which are based on those in [7].

This work was supported in part by the U.S. Department of Energy's Office of Energy Efficiency and Renewable Energy (EERE) through Solar Energy Technologies Office (SETO), under Grant 38637 (UNIFI consortium).

979-8-3315-8138-1

These models include inner current and outer voltage control loops, LCL output filters, and primary control schemes. The diesel generator (DG) on feeder 1 has a capacity of 4,000 kVA, and is modeled using the GENTPJ model—a reduced-order two-axis model of a round rotor salient pole generator [8]. The GFM inverter on feeder 2 is droop-based and has a capacity of 3,000 kVA.

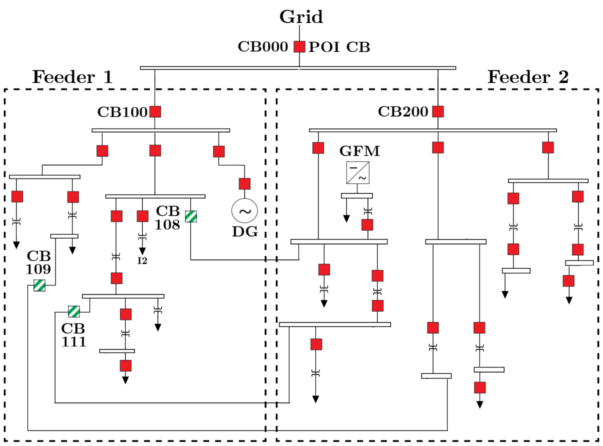

Fig. 1: An abridged two-feeder version of the Banshee microgrid. Normally open CBs are striped green, and normally closed CBs are red.

B. Linearized Model

Our suite of controls can be used to open and close certain CBs in the system, changing the mode and system topology as seamlessly as possible. Additionally, the suite of controls has intra-mode controls such as active power tie-line control and frequency regulation. However, due to the complexity of the system, it is often difficult to choose controller gains and guarantee stability for the full-order nonlinear model. To facilitate this task, we simplify the model as shown in Fig. 2. The resulting model comprises one CB connecting each feeder to the grid, one CB connecting feeder 1 to feeder 2, and one CB acting as the POI with the grid. The loads on each feeder are aggregated into one load per feeder. In addition, we make the following assumptions:

A1 The microgrid is balanced and operating in sinusoidal regime.

A2 There is one short and lossless transmission line connecting feeders 1 and 2 through CB111.

A3 System voltage magnitudes in each mode are treated as constant, under the assumption that the voltage controls in the system work faster than those for frequency.

A4 The system is linearized using the following approximation: $\sin(\theta_i - \theta_j) \approx \theta_i - \theta_j$.

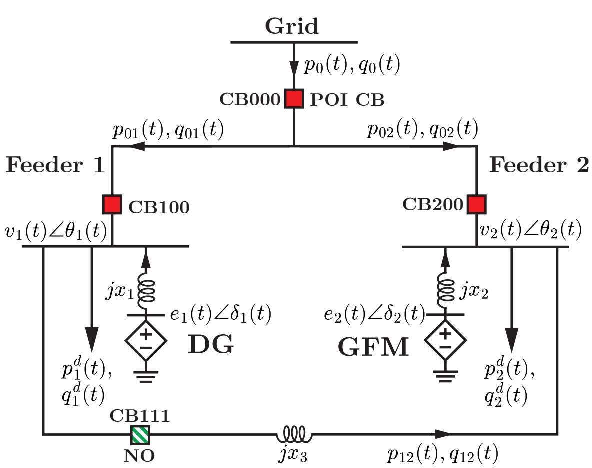

Fig. 2: The simplified model of the abridged Banshee system.

We model the generating resources using a voltage behind the reactance model. Let $v_i(t)$ and $\theta_i(t)$ respectively denote the magnitude and phase angle at time t of the phasor associated with the voltage at bus $i = 1, 2$. Additionally, let $e_i(t)$ and $\delta_i(t)$ respectively denote the magnitude and phase angle at time t of the phasor associated with the internal voltage of the generator connected at bus $i = 1, 2$. In addition, let $\Delta\omega_i(t)$ denote the difference between the frequency measurement at the generator on feeder i, at time t, and the nominal frequency, $\omega_0 = 2\pi 60$ rad/sec. Furthermore, define $p_i^r(t)$ to be the active power reference command given to the generating resource on feeder i, and $p_i^g(t)$ to be the active power injection of the generating resource on feeder i. Then, the evolution of $\delta_i(t),\ i = 1, 2$, is governed by

$$\begin{aligned}
\frac{d\delta_1(t)}{dt} &= \Delta\omega_1(t), \\
J_1 \frac{d\Delta\omega_1(t)}{dt} &= p_1^r(t) - p_1^g(t) - \frac{1}{R_1\omega_0}\Delta\omega_1(t), \\
\frac{d\delta_2(t)}{dt} &= \Delta\omega_2(t), \\
H_2 \frac{d\Delta\omega_2(t)}{dt} &= p_2^r(t) - p_2^g(t) - D_2\Delta\omega_2(t),
\end{aligned}$$

where $J_1\ \left[\frac{\mathrm{s}^2}{\mathrm{rad}}\right]$ is the inertia constant of the DG, $R_1\ \left[\mathrm{pu}\right]$ is the regulation constant of the DG, $H_2\ \left[\frac{\mathrm{s}^2}{\mathrm{rad}}\right]$ is a small parameter, and $D_2\ \left[\frac{\mathrm{s}}{\mathrm{rad}}\right]$ is the droop coefficient of the GFM inverter. As voltage is treated as a constant in this model, we disregard the reactive power/voltage primary control equations.

III. Controls

The suite of controls implemented in the Banshee model includes active power tie-line regulation across the POI and between the two feeders when they are connected through CB111. Additionally, the system can island and re-synchronize individual feeders from/to the grid, disconnect two previously interconnected feeders, and synchronize islanded feeders to form a single microgrid. Finally, when the feeders are islanded from the grid, secondary frequency regulation can be activated. A description of each of these controls along with their labeling is provided in Table I. While our controls are applied to a two feeder system, the control architecture proposed in this paper can be extended to other microgrids.

A. System Mode Description

When a CB is opened or closed, the network topology changes; we refer to each distinct topology as a mode. The

979-8-3315-8138-1

TABLE I: System Controls

Note: $i, j \in \{1, 2\},\ i \neq j$, and subscripts for the variables involving feeders i and j are not ordered (i.e., $u_{ij} = u_{ji}$).

Control	Description	Enable	$z_n(t)$	κ_n	$\varepsilon_n(t)$
u_0^p	Active power regulation across the POI CB.	$\tau_0^p(t)$	$\mu_0^p(t)$	α_0^p	$(p_0(t) - p_0^*(t))\, \tau_0^p(t)$
u_{0i}	Disconnection of feeder i from the grid.	$\tau_{0i}(t)$	$\mu_{0i}^p(t)$	α_{0i}^p	$(p_{0i}(t) - 0)\, \tau_{0i}(t)$
u_{ij}^p	Active power regulation across the CB connecting feeders i and j.	$\tau_{ij}^p(t)$	$\mu_{ij}^p(t)$	α_{ij}^p	$\left(p_{ij}(t) - p_{ij}^*(t)(1-\tau_{ij})\right) \left(\tau_{ij}^p(t) + \tau_{ij}(t)\right)$
u_{ij}	Disconnection of feeders i and j.	$\tau_{ij}(t)$			
$\bar{u}_{0i}$	Synchronization of feeder i to the grid.	$\sigma_{0i}(t)$	$\nu_{0i}^p(t)$	λ_{0i}^p	$(\theta_{0i}(t) - 0)\, \sigma_{0i}(t)$
$\bar{u}_{ij}$	Synchronization of feeders i and j.	$\sigma_{ij}(t)$	$\nu_{ij}^p(t)$	λ_{ij}^p	$(\theta_{ij}(t) - 0)\, \sigma_{ij}(t)$
u_i^p	Frequency regulation on feeder i.	$\xi_i^p(t)$	$\eta_i^p(t)$	β_i^p	$(\Delta\omega_i(t) - 0)\, \xi_i^p(t)$

system depicted in Fig. 3 has a total of seven desired modes. We denote the modes as follows: grid connected (GC), partially islanded 1 (PI1), partially islanded 2 (PI2), fully islanded (FI), backfed 1 (BF1), backfed 2 (BF2), and networked (NW). Note that for all desired modes the POI CB is closed and it only opens for unintentional disturbances, which are not addressed in this paper. It is more desirable to island at the feeder level (CB100, CB200) than the POI in order to have more direct control over each feeder. Additionally, no desired mode topology contains loops.

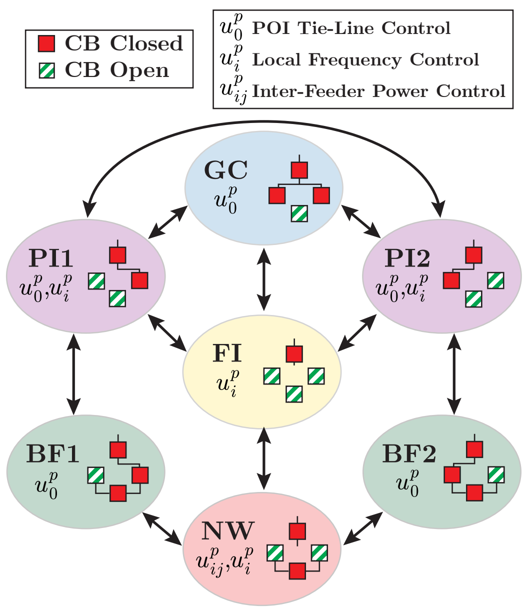

Fig. 3: The 7 desired modes of the Banshee distribution system. The controls listed within each mode can be activated without triggering a mode transition.

Figure 3 depicts the possible transitions among modes, as well as the possible controls active within each of the seven modes. Let s_{00}, s_{10}, s_{20} and s_{12} denote indicator variables associated with CB's CB000, CB100, CB200, and CB111, respectively, with each taking value 1 when the corresponding CB is closed, and 0 otherwise. Then, we can define:

$$m_{GC} = s_{00}s_{10}s_{20}(1 - s_{12}), \tag{1}$$

$$m_{PI1} = s_{00}(1 - s_{10})s_{20}(1 - s_{12}), \tag{2}$$

$$m_{PI2} = s_{00}s_{10}(1 - s_{20})(1 - s_{12}), \tag{3}$$

$$m_{FI} = s_{00}(1 - s_{10})(1 - s_{20})(1 - s_{12}), \tag{4}$$

$$m_{BF1} = s_{00}(1 - s_{10})s_{20}s_{12}, \tag{5}$$

$$m_{BF2} = s_{00}s_{10}(1 - s_{20})s_{12}, \tag{6}$$

$$m_{NW} = s_{00}(1 - s_{10})(1 - s_{20})s_{12}; \tag{7}$$

each of these is equal to 1 when the system is in the mode indicated by the labels in the sub-indices, and 0 otherwise.

Additionally, in column 3 of Table I we present a binary indicator variable that can be used to enable/disable each control. In column 4 of Table I we list an internal control variable, $z_n(t)$, for each of the integral controllers in the system, where $n = 1, 2, ..., 9$. In columns 5 and 6 of Table I we list the integral controller gain, κ_n, and the input/error term, $\varepsilon_n(t)$ for the controllers. Define $p_i^*(t)$ as an external reference setpoint for generating resource i, and let $p_{12}^*(t)$ and $p_0^*(t)$ denote the active power reference setpoints for the power flow across CB111 and CB000 respectively. We define power flowing into the microgrid is as positive. Then, we can define a generic integral function for all controllers in the system as:

$$\dot{z}_n(t) = \kappa_n \varepsilon_n(t), \tag{8}$$

$$p_i^r(t) = p_i^*(t) + \sum_{n=1}^{9} \rho_{i,n} z_n(t), \quad i = 1, 2, \tag{9}$$

where $\rho_{i,n} \in (0, 1)$ is the participation factor associated with generator i and controller n. Note that not all controllers can be active for each mode, and not all controllers can be active simultaneously.

B. Closed-Loop State-Space Model

Next, we introduce a state-space model for the linearized Banshee system. Let $p_0(t), p_{01}(t), p_{02}(t)$ denote the power flows across CB100, CB200, and CB111, respectively. Also, define $\theta_{ij}(t) = \theta_i(t) - \theta_j(t)$. Finally, let $p_i^d(t)$ denote the active power load on feeder i. In the remainder of the paper we suppress the time argument in all variables for ease of notation. Define,

$$x_p = \begin{bmatrix} \delta_1 & \Delta\omega_1 & \delta_2 & \Delta\omega_2 \end{bmatrix}^\top,$$

$$u_p = \begin{bmatrix} p_1^r & p_2^r \end{bmatrix}^\top,$$

$$d_p = \begin{bmatrix} p_1^d & p_2^d \end{bmatrix}^\top,$$

$$x_c = \begin{bmatrix} \mu_0^p & \mu_{01}^p & \mu_{02}^p & \mu_{12}^p & \eta_1^p & \eta_2^p & \nu_{01}^p & \nu_{02}^p & \nu_{12}^p \end{bmatrix}^\top,$$

$$u_c = \begin{bmatrix} p_0 & p_{01} & p_{02} & \Delta\omega_1 & \Delta\omega_2 & \theta_{01} & \theta_{02} & \theta_{12} \end{bmatrix}^\top,$$

979-8-3315-8138-1

$d_c = \begin{bmatrix} p_1^* & p_2^* \end{bmatrix}^\top.$

Then, the state-space model for the closed-loop model is given by,

$$E_p\dot{x_p} = A_p x_p + B_p u_p, \tag{10}$$
$$u_p = C_c x_c, \tag{11}$$
$$\dot{x_c} = B_c u_c + F_c d_c, \tag{12}$$
$$u_c = C_p x_p + H_p d_p. \tag{13}$$

By substituting (11) into (10) and substituting (13) into (12) we obtain:

$$\underbrace{\begin{bmatrix} E_p & \mathbb{0} \\ \mathbb{0} & \mathbb{I} \end{bmatrix}}_{E_f}\underbrace{\begin{bmatrix} \dot{x_p} \\ \dot{x_c} \end{bmatrix}}_{\dot{x}_f} = \underbrace{\begin{bmatrix} A_p & B_pC_c \\ B_cC_p & \mathbb{0} \end{bmatrix}}_{A_f}\underbrace{\begin{bmatrix} x_p \\ x_c \end{bmatrix}}_{x_f} + \underbrace{\begin{bmatrix} \mathbb{0} & \mathbb{0} \\ B_cH_p & F_c \end{bmatrix}}_{F_f}\underbrace{\begin{bmatrix} d_p \\ d_c \end{bmatrix}}_{d_f}. \tag{14}$$

where $\mathbb{0}$ and $\mathbb{I}$ respectively denote a zero matrix and identity matrix of appropriate dimensions. The state-space model is a function of the system mode and the controls active at any given time. Due to space constraints, we do not provide the expressions for the A_f and F_f matrices. However, they can be derived using the integral control equations and reference values in (9) and (8), the mode-dependent power flow equations derived from Fig. 2, and the indicator variables in (1)-(7).

IV. Controller Gain Choice

In this section, we choose controller gains, k_m, as listed in column 5 of Table I that make (14) stable for the parameter values listed in Table II. These parameters were extracted from the full-order model of the Banshee system, and are given in per unit unless otherwise specified. As each mode in the system comprises a different network topology, a power flow formulation was executed for each mode to determine the value of v_1 and v_2. Note that despite the different topologies, all v_1 and v_2 values are respectively within 2.75×10^{-5} pu and 3.70×10^{-4} pu of one another. In addition, the values of e_1, e_2, v_1 and v_2 are approximately 1.03 pu due to small internal generator reactances, x_1 and x_2.

A. Open-Loop Stability Analysis

We use the matrices E_p and A_p from (10) to examine the stability of the open-loop system model [9]. Define $\mathbb{e}_1 = \begin{bmatrix} 1 & 0 \end{bmatrix}^\top$ and $\mathbb{e}_2 = \begin{bmatrix} 0 & 1 \end{bmatrix}^\top$. Let G_i denote the kronecker product of the 2-dimensional identity matrix and $\mathbb{e}_i$. Additionally, define the following matrices,

$$S_1 = \begin{bmatrix} s_{10} & 0 \\ 0 & s_{20} \end{bmatrix} \text{ and } M = \begin{bmatrix} 1 \\ -1 \end{bmatrix}.$$

Let $\gamma_1 = \frac{v_1 e_1}{x_1}$, $\gamma_2 = \frac{v_2 e_2}{x_2}$, $\gamma_{12} = \frac{v_1 v_2}{x_3}$, and

$$\Gamma = -\left[\begin{array}{cc|cc} -\gamma_1 & 0 & \gamma_1 & 0 \\ 0 & -\gamma_2 & 0 & \gamma_2 \\ \hline \gamma_1 & 0 & -\gamma_1 - \gamma_{12}s_{12} & \gamma_{12}s_{12} \\ 0 & \gamma_2 & \gamma_{12}s_{12} & -\gamma_2 - \gamma_{12}s_{12} \end{array}\right],$$

$$= -\left[\begin{array}{c|c} \Gamma_{11} & \Gamma_{12} \\ \hline \Gamma_{21} & \Gamma_{22} \end{array}\right].$$

While A_p is dependent on the mode and network topology, define the mode-agnostic element of A_p to be

$$A = \begin{bmatrix} 0 & 1 & 0 & 0 \\ 0 & -\frac{1}{R_1\omega_0} & 0 & 0 \\ 0 & 0 & 0 & 1 \\ 0 & 0 & 0 & -D_2 \end{bmatrix}, \text{ and } E_p = \begin{bmatrix} 1 & 0 & 0 & 0 \\ 0 & J_1 & 0 & 0 \\ 0 & 0 & 1 & 0 \\ 0 & 0 & 0 & H_2 \end{bmatrix}.$$

Then, we define A_p to be:

$$A_p = A + G_2\Big((1 - s_{12})S_1\Gamma_{11} - s_{12}\gamma_{12}MM^\top\Big)G_1^\top.$$

The coefficients of the characteristic polynomial for each mode in open loop, given by $\det(sE_p - A_p) = 0$, are presented in Table III. Note that for modes PI1, PI2, FI, and NW, E_p and A_p must be modified to remove the zero eigenvalue that appears when a second reference angle is introduced to the system. Furthermore, for FI this modification is used to remove two zero eigenvalues. By applying the Routh-Hurwitz criterion, we determine that the system is open-loop stable in all modes [10].

B. Closed-Loop Stability Analysis

In the closed-loop model in (14), while the matrix E_f is constant, the matrix A_f is a function of both the mode/system topology, as well as the controls active at any given time. As an example, the entry (5,1) of the matrix A_f can be shown to be:

$$\tau_0^p\alpha_0^p\overline{m}\Big(\mathbb{e}_1^\top\Gamma_{11}\overline{m} - (\mathbb{e}_1^\top S_{BF1} + \mathbb{e}_2^\top S_{BF2})\Gamma_{12}\Gamma_{22}^{-1}\Gamma_{21}\Big)\mathbb{e}_1,$$

where

$$\overline{m} = m_{GC} + m_{PI1} + m_{PI2} + m_{BF1} + m_{BF2}.$$

When the system is in GC mode and active power POI control is enabled, A_f (which includes the above term) is a function of α_0^p:

$$A_f = \begin{bmatrix} 0 & 1 & 0 & 0 & 0 \\ -6475.57 & -0.053 & 0 & 0 & 0.5 \\ 0 & 0 & 0 & 1 & 0 \\ 0 & 0 & -482.11 & -0.053 & 0.5 \\ -6475.57\alpha_0^p & 0 & -482.11\alpha_0^p & 0 & 0 \end{bmatrix},$$

where rows/columns 6-13 have been omitted as no other controls are active and those rows are therefore unnecessary. Figure 4 depicts the 5 eigenvalues of the descriptor state-space as we sweep across values of α_0^p from -100 to 500. Based on the position of the eigenvalues where they enter the OLHP, the constraints on α_0^p are $0 < \alpha_0^p \leq 52.55$.

TABLE II: Primary Control System Parameters.

Initial Conditions	x_1	x_2	x_3	p_1^*	p_2^*	p_1^d	p_2^d	q_1^d	q_2^d	e_1, e_2 v_1, v_2	J_1	R_1	H_2	D_2
Value	1.6×10^{-4}	0.002	0.178	0.146	0.125	0.185	0.166	0.090	0.081	1.03	0.002	0.05	0.0001	0.053

TABLE III: Characteristic Polynomial Coefficients

	a_4	a_3	a_2	a_1	a_0
GC	1.0	557	8.10×10^6	1.86×10^9	1.58×10^{13}
PI1	–	1.0	557	4.83×10^6	1.29×10^8
PI2	–	1.0	557	3.28×10^6	1.73×10^9
FI	–	–	1.0	557	1.42×10^4
BF1	1.0	557	4.83×10^6	1.31×10^8	1.43×10^{10}
BF2	1.0	557	3.34×10^6	1.74×10^9	1.93×10^{11}
NW	–	1.0	557	7.61×10^4	3.15×10^6

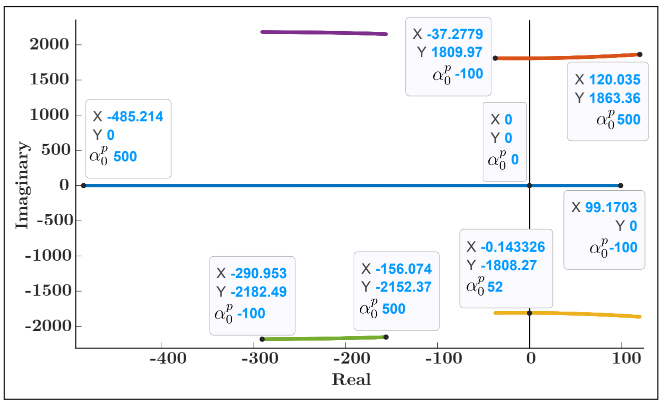

Fig. 4: The modes of the closed-loop system in GC mode with active power POI control has been enabled.

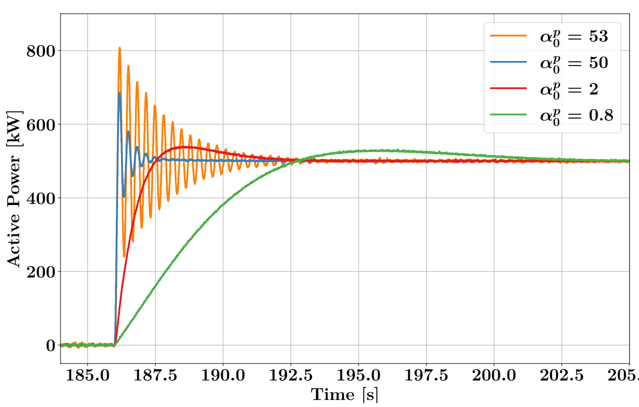

Fig. 5: Various gain values for active power POI control tested on the full order Banshee system in GC mode.

V. Simulation/Application of Control Gains

In this section we test various values of α_0^p on the full-order Banshee system model, implemented in a real-time C-HIL testbed. Figure 5 depicts the response of the system with varying gain values to a change in the reference setpoint p_0^*. The simulation begins with the system in GC mode with $\tau_0^p = 1$, and power across CB000 at 0 kW. Then, at time $t = 186$ s the reference p_0^* changes to 500 kW and the generators on feeders 1 and 2 are dispatched to track the reference. The participation factor for each resource is 0.5. The full order Banshee system remains stable when $0 < \alpha_0^p < 58$, which is a slightly larger range than that of the linearized system. However, as α_0^p increases (especially past 52.55), the system response becomes increasingly oscillatory and undesirable. While there is a slight mismatch in the regions of stability between the two models, the linearized model is more conservative.

VI. Concluding Remarks

In this paper, we consider an abridged version of the Banshee microgrid equipped with a suite of controllers that can seamlessly transition the system through seven operating modes. To characterize regions of stability for the full-order model throughout different modes and possible controls, we analyze a linearized closed-loop state space model of the system. Simulation results illustrate that tuning the linearized system is helpful in characterizing stable and unstable regions of operation. While the regions of stability for the full-order model and the linearized model may not overlap exactly, those of the linearized model are often more conservative. Future work aims to relax assumptions made regarding voltage, lossless lines, small angle approximations, and disturbances.

References

[1] R. Salcedo, E. Corbett, C. Smith, E. Limpaecher, R. Rekha, J. Nowocin *et al.*, "Banshee distribution network benchmark and prototyping platform for hardware-in-the-loop integration of microgrid and device controllers," *The J. of Eng.*, vol. 2019, no. 8, pp. 5365–5373, 2019.

[2] J. Wang, A. Pratt, M. Baggu, and C. Zhao, "Design of an advanced energy management system for microgrid control using a state machine," *Appl. Energy*, vol. 228, pp. 2407–2421, 2018.

[3] C. Sun, G. Joos, S. Q. Ali, J. N. Paquin, C. M. Rangel, F. A. Jajeh *et al.*, "Design and real-time implementation of a centralized microgrid control system with rule-based dispatch and seamless transition function," *IEEE Trans. on Industry Appl.*, vol. 56, no. 3, pp. 3168–3177, 2020.

[4] T. M. L. Assis and G. N. Taranto, "Automatic reconnection from intentional islanding based on remote sensing of voltage and frequency signals," *IEEE Trans. on Smart Grid*, vol. 3, no. 4, pp. 1877–1884, 2012.

[5] A. Micallef, M. Apap, C. Spiteri-Staines, and J. M. Guerrero, "Single-phase microgrid with seamless transition capabilities between modes of operation," *IEEE Trans. on Smart Grid*, vol. 6, no. 6, pp. 2736–2745, 2015.

[6] Y. Du, H. Tu, S. Lukic, D. Lubkeman, A. Dubey, and G. Karsai, "Development of a controller hardware-in-the-loop platform for microgrid distributed control applications," in *IEEE Electron. Power Grid*, 2018, pp. 1–6.

[7] O. Ajala, "A hierarchy of microgrid models with some applications," Ph.D. dissertation, University of Illinois Urbana-Champaign, 2018.

[8] M. S. Islam, G. Laera, M. de Castro Fernandes, L. Vanfretti, C. Mishra, and K. Jones, "Modeling specialized electric power generators, excitation systems and prime movers used by north american utilities," Oct. 2023.

[9] A. Varga, "On stabilization methods of descriptor systems," *Syst. & Control Letters*, vol. 24, no. 2, pp. 133–138, 1995.

[10] M. F. Golnaraghi and B. C. Kuo, *Autom. Control Syst.* McGraw-Hill Education, 2017.

979-8-3315-8138-1